*36th EPS Conference on Plasma Phys. Sofia, June 29 - July 3, 2009 ECA Vol.**33E**, P-1.158 (2009)*

Impurity Transport within an ELM-cycle at the Edge Transport Barrier in ASDEX Upgrade

T. Pütterich, R. Dux, E. Wolfrum, E. Viezzer and the ASDEX Upgrade Team

Max-Planck-Institut für Plasmaphysik, EURATOM Assoc., D-85748 Garching, Germany

In H-mode plasmas the turbulent transport of energy and particles is strongly suppressed in a thin radial region at the edge of the confined plasma. The width of this edge transport barrier (ETB) is rather small (for ASDEX Upgrade < 2 cm) with large radial gradients for T_e, T_i and n_e. For ELMy H-modes, edge-localized modes (ELMs) occur which make the steep gradients of temperature and density collapse for a few 100 microseconds. These recover again in the following milliseconds until the next ELM occurs. The details of this barrier determine how well the plasma confines energy enhancing its performance and how well it confines impurities and He ash which, in general, reduces the performance of a fusion plasma. The small spatial extent of the barrier and the fast change due to ELMs requires a diagnostic with good spatial and temporal resolution. In [1] the transport of C^{6+} has been investigated and model functions for radial diffusion coefficients and drift velocities arrived at the best match between modelled and measured C^{6+}-density profiles for values which resemble the neoclassical transport coefficients at the ETB. The neoclassical inward drift was observed in the ETB region, where the diffusion coefficient is reduced to the neoclassical, low values. In [2,3] it has also been found by analyses of soft X-ray radiation, that for Ne and F the transport in the ETB is close to the neoclassical values. In this work, the diffusion coefficients and inward pinches for He^{2+}, C^{6+}, Ne^{10+} and Ar^{16+} during the inter-ELM phase are measured and compared to the neoclassical values to gather further experimental evidence on the ETB transport. The ELM itself is not subject of these investigations.

Experiment

In ASDEX Upgrade H-mode discharges with a plasma current of $1\,\mathrm{MA}$ and a magnetic field on axis of $2.5\,\mathrm{T}$ have been performed to study the ETB transport. An ELM frequency of about 60 Hz is obtained with $2.5\,\mathrm{MW}$ beam heating and $1.6\,\mathrm{MW}$ ECRH heating, while a feed-forward gas puff of $7 \cdot 10^{21}\,\mathrm{s}^{-1}$ is applied to keep the ELM frequency stable. The radial plasma position is scanned by about $15\,\mathrm{mm}$ to provide good edge measurements on electron temperature and density and to optimize the measurements from the edge CXRS system. In this setup the density of the intrinsic impurities He^{2+} and C^{6+} are determined. For the impurities Ne^{10+} and Ar^{16+}, the discharges have been repeated and non-perturbative Ne and Ar puffs are applied such that for a short phase of $600\,\mathrm{ms}$ a constant impurity concentration of $1 \cdot 10^{-3}$ (Ne) and $5 \cdot 10^{-4}$ (Ar) is obtained at the pedestal-top. Slight modifications of the ELM frequency are observed, but their impact on the results of the analysis are minor as the analysis suggests that the impurity transport before and after an ELM is nearly equal (s. below). In fig. 1 the T_e-, T_i- and n_e-profiles are presented. The ELM itself disturbs the profiles, but already 2 ms after the ELM the profiles become similar to those just before the ELM (compare left to right column in fig. 1). This is reflected by the neoclassical transport coefficients which exhibit similar diffusion coefficients and inward pinches at both time points. The drift velocities are only reduced by 10-20%. These flux surface averaged transport coefficients are calculated by NEOART [4,5] and are presented in the lower part of fig. 2. The variations for the two time points and uncertainties resulting from uncertain impurity concentrations are indicated by the two black curves for each profile of the transport coefficients in the lower part of fig. 2.

For the determination of the transport coefficients the impurity concentrations from the real experiments were used, i.e. for determining the coefficients for He and C neither Ne or Ar were present, while for the coefficients of the two noble gases either gas type was added to the natural impurity mix. The impurity concentrations used are 5-25% He, 1% C, $3 \cdot 10^{-3}$ O and $1 \cdot 10^{-5}$ W. The background density gradient and the other impurities lead to a neoclassical inward drift for an impurity species, which increases with the local charge state of the impurity. The typical time scale for the neoclassical transport across the about 1-2 cm wide pedestal region is for diffusion and convection in the range of 1 ms, which is short compared to the ELM repetition time of about 15 ms. The problem is complicated by the presence of turbulent transport in the vicinity of the ETB and by the question how well and in what radial shape the turbulence is suppressed. The alignment of the T_e-, T_i- and n_e-profiles and the separatrix position is determined by shifting the individual experimental profiles by less than 5 mm, while the Thomson scattering data allows to relatively align the T_e- and n_e-profiles unambiguously. The T_i-profiles are then shifted to match the pedestal position observed in T_e. The separatrix position is attributed such that the power balance is matched as described in [6]. It should be noted that the measurements of the intensity profiles of the CX-emission are connected to the T_i-profiles as both quantities are obtained from the same CXRS-spectrum. A more detailed description of the adjustments and the edge CXRS system can be found in [7]. The impurity density profiles are then derived from the intensities using the atomic data from the ADAS project [8], which considers effective cross sections, beam attenuation and excitation.

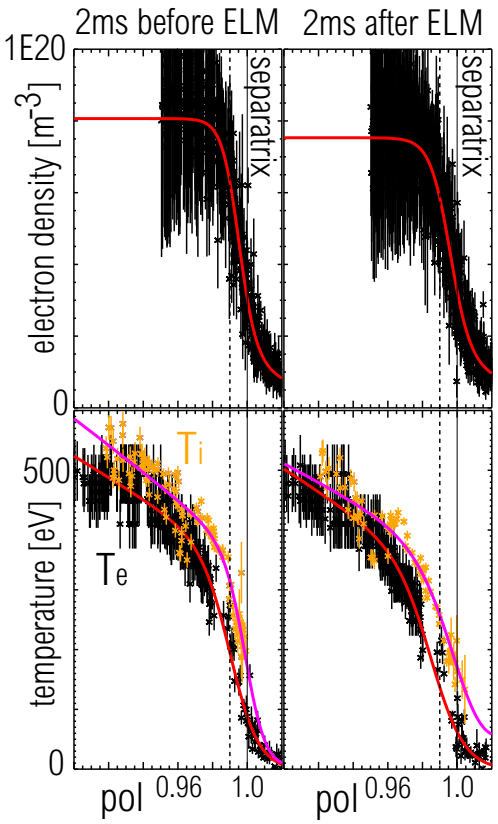

Fig. 1: *T_e-, T_i- and n_e-profiles before and after an ELM as measured during the analysed discharge phase.*

Modelling with 1D-Transport code STRAHL

The evolution of the He^{2+}-, C^{6+}-, Ne^{10+}- and Ar^{16+}-density profiles is modelled with the impurity transport code STRAHL [4], which takes into account ionization and recombination rates and calculates time-dependently the densities of all ionization stages along the plasma radius in a flux surface averaged manner. The local ionization and recombination rates (taken from ADAS) are evaluated by taking the measured electron profiles into account. The impurity transport is treated using a flux surface averaged diffusion coefficient D and drift velocity v profile, which is constant in the inter-ELM phase. In the actual case, 100 ELM cycles were simulated, while a constant impurity influx is assumed. Within the simulated 100 ELM cycles the impurity densities arrive at a quasi-equilibrium, which is modulated by the ELMs. The quasi-equilibrium depends on the transport coefficients and the chosen impurity influx. In the model, the effects of an ELM are resembled by increasing D ($10\,m^2\,s^{-1}$, s. fig. 2) for $200\mu s$ at the pedestal region, while the transport in-between ELMs is set to a time-independent profile, as presented in the lower part of fig. 2. The turbulent transport (here estimated to be

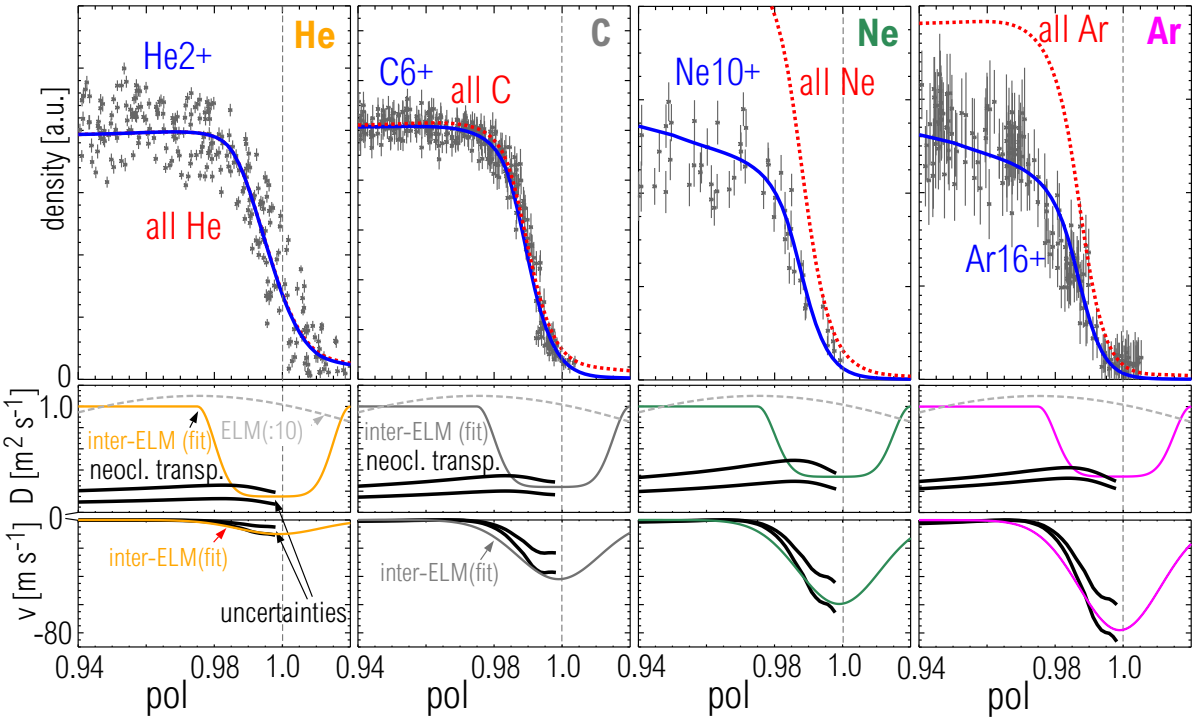

Fig. 2: *Measured impurity density profiles along with the best fit of modelled profiles.*

$1\,\mathrm{m^2\,s^{-1}}$) is assumed to be dominant up to the normalized (poloidal magnetic flux) coordinate $\rho_{pol} = 0.975$, from where it decays to a value which is determined by a least square fit, which compares the measured to the modelled profiles of He^{2+}-, C^{6+}-, Ne^{10+}- and Ar^{16+}. Outside the separatrix the diffusion coefficient is increased again to the turbulent level. This outer region is not subject of this work, as the CXRS measurements are there not available for all impurities and the parallel transport to the divertor requires special attention. For the pinch velocity a Gaussian dip is assumed at $\rho_{pol} = 0.999$ and a Gaussian width of 0.012. The maximum pinch velocity is subject to the least square fit. Elsewhere the pinch velocity is assumed to be 0. The values (such as the width and position of the Gaussian dip in v), which are not subject to the least-square fit are in accordance to the findings presented in [1], where dedicated parameter scans have been performed to find the best least-square fit for these parameters in the case of C^{6+}. The investigations on C^{6+} give the best information on these parameters, because the data quality is best and the C^{6+}-gradient matches the position of the inward pinch, while for He^{2+}, Ne^{10+} and Ar^{16+}, the ionization equilibrium in combination with the transport brings the gradients to positions where less information can be obtained.

Results and Discussion

In fig. 2, the results are presented for all four impurities. The data points originate from the inter-ELM phases, i.e. excluding the intervall 2 ms before to 5 ms after the ELM. As described above, the profiles should be close to the equilibrium value and indeed form a continuous profile if statistical uncertainties are taken into account. For He, the scatter of the data points are larger than the statistical uncertainties. Possibly this is due to disturbances in the impurity densities at the edge, which get more obvious for lower ionization stages. In each part of fig. 2, the modelled ion densities and total impurity density are depicted resulting from the best fit of the transport coefficients. The fit was done between $0.96 < \rho_{pol} < 1.00$ to put special emphasis on the ETB region. To some extent v and D can be separated by the analysis as the value of v influences the position of the pedestal in impurity

density and v/D the steepness of the gradient. The size of v and D can also be determined by including the evolution of the profiles similar to [1]. However, the data quality for the other impurities does not yield an improvement of the results when doing this analysis. In the lower part of fig. 2, the inter-ELM transport profiles used to obtain the fits to the impurity densities are presented in color along with the black curves which represent the neoclassical transport coefficients and their uncertainties. The error bars on the fitted profiles are indicated in fig. 3. There, the fit results for D and v are compared to the neoclassical transport coefficients at $\rho_{pol} = 0.99$. Additionally, the peaking factor

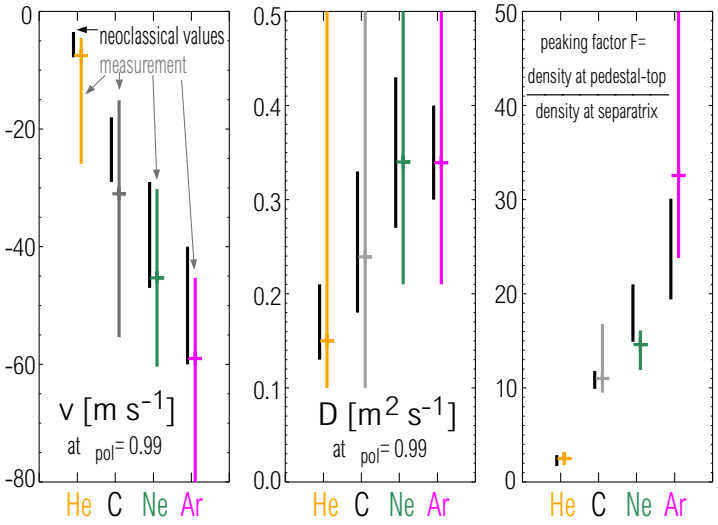

Fig. 3: *v and D values at $\rho_{pol} = 0.99$ as fitted and neoclassical values. The peaking factor F is presented to give a comparison about the integrated effect of the v and D profiles.*

$$F = \frac{n_I(\rho_{pol} = 0.97)}{n_I(\rho_{pol} = 1.0)} = exp[\int_{\rho_{pol}=1.0}^{\rho_{pol}=0.97} \frac{v}{D} dr]$$

is presented which summarizes the integrated effect of the transport coefficient profiles. While v and D are in agreement with the neoclassical values, relatively large uncertainties exist. As v/D is much less uncertain the comparision of the peaking factor F from neoclassical values compared to the fitted values can be understood as quite good confirmation of the model that the pedestal in impurity densities is governed by neoclassical transport. It should be noted, that if for the fit D is prescribed, the analysis gives unambiguously v, which is in agreement with the neoclassical value with relatively small error bars. As predicted the inward pinch and therefore the peaking factor F is increasing with the charge of the impurity species. For tungsten, this trend would suggest a peaking factor at the pedestal between 65 and 140. This strong effect emphasizes the importance of high ELM-frequencies to control the impurities of high-Z elements as found in [9–11].

References

[1] T. Pütterich et al., EPS 2008,Hersonissos, Crete, P-2.083
[2] R. Dux, Fusion Science and Technology **44**, 708 (2003)
[3] T. Sunn Pedersen et al., Nucler Fusion **40**, 1795 (2000)
[4] R. Dux, Technical Report No. 10/30, IPP, Garching, Germany (2006)
[5] A. G. Peeters, provided the NEOART code (1998)
[6] J. Neuhauser et al., PPCF **44**, 855 (2002)
[7] T. Pütterich et al., PRL **102**, 025001 (2009)
[8] H. P. Summers, ADAS User Manual v2.6, http://adas.phys.strath.ac.uk (2004)
[9] R. Neu et al, EPS 2003,St. Petersburg, Russia, P-1.123
[10] R. Dux et al, Jour. Nucl. Mat. 390-391, 858 (2009)
[11] R. Dux et al, this conference, O-5.056